

Measurement of the branching fraction for the decay $K_S \rightarrow \pi \mu \nu$ with the KLOE detector

The KLOE-2 Collaboration

D. Babusci^d, M. Berlowski^v, C. Bloise^d, F. Bossi^d, P. Branchini^s,
A. Budano^{r,s}, B. Cao^u, F. Ceradini^{r,s}, P. Ciambone^d, F. Curciarello^{a,d},
E. Czerwiński^c, G. D'Agostini^{n,o}, E. Danè^d, V. De Leo^{n,o}, E. De Lucia^d,
A. De Santis^d, P. De Simone^d, A. Di Cicco^{r,s}, A. Di Domenico^{n,o},
D. Domenici^d, A. D'Uffizi^d, A. Fantini^{p,q}, P. Fermani^d, S. Fiore^{t,o}, A. Gajos^c,
P. Gauzzi^{n,o}, S. Giovannella^d, E. Graziani^s, V. L. Ivanov^{g,h}, T. Johansson^u,
X. Kang^d, D. Kisielewska-Kamińska^c, E. A. Kozyrev^{g,h}, W. Krzemien^v,
A. Kupsc^u, P. A. Lukin^{g,h}, G. Mandaglio^{f,b}, M. Martini^{d,m}, R. Messi^{p,q},
S. Miscetti^d, D. Moricciani^d, P. Moskal^c, S. Parzych^c, A. Passeri^s, V. Patera^{l,o},
E. Perez del Rio^{n,o}, P. Santangelo^d, M. Schioppa^{j,k}, A. Selce^{r,s,*}, M. Silarski^c,
F. Sirghi^{d,e}, E. P. Solodov^{g,h}, L. Tortora^s, G. Venanzoniⁱ, W. Wiślicki^v,
M. Wolke^u

^a*Dipartimento di Fisica e Astronomia "Ettore Majorana", Università di Catania, Italy*

^b*INFN Sezione di Catania, Catania, Italy.*

^c*Institute of Physics, Jagiellonian University, Cracow, Poland.*

^d*Laboratori Nazionali di Frascati dell'INFN, Frascati, Italy.*

^e*Horia Hulubei National Institute of Physics and Nuclear Engineering, Măgurele, Romania*

^f*Dipartimento di Scienze Matematiche e Informatiche, Scienze Fisiche e Scienze della Terra dell'Università di Messina, Messina, Italy.*

^g*Budker Institute of Nuclear Physics, Novosibirsk, Russia.*

^h*Novosibirsk State University, Novosibirsk, Russia.*

ⁱ*INFN Sezione di Pisa, Pisa, Italy.*

^j*Dipartimento di Fisica dell'Università della Calabria, Rende, Italy.*

^k*INFN Gruppo collegato di Cosenza, Rende, Italy.*

^l*Dipartimento di Scienze di Base ed Applicate per l'Ingegneria dell'Università "Sapienza", Roma, Italy.*

^m*Dipartimento di Scienze e Tecnologie applicate, Università "Guglielmo Marconi", Roma, Italy.*

ⁿ*Dipartimento di Fisica dell'Università "Sapienza", Roma, Italy.*

^o*INFN Sezione di Roma, Roma, Italy.*

^p*Dipartimento di Fisica dell'Università "Tor Vergata", Roma, Italy.*

^q*INFN Sezione di Roma Tor Vergata, Roma, Italy.*

^r*Dipartimento di Matematica e Fisica dell'Università "Roma Tre", Roma, Italy.*

^s*INFN Sezione di Roma Tre, Roma, Italy.*

^t*ENEA, Department of Fusion and Technology for Nuclear Safety and Security, Frascati (RM), Italy*

^u*Department of Physics and Astronomy, Uppsala University, Uppsala, Sweden.*

^v*National Centre for Nuclear Research, Warsaw, Poland.*

*Corresponding author

Email address: andrea.selce@roma3.infn.it (A. Selce)

Abstract

Based on a sample of 300 million K_S mesons produced in $\phi \rightarrow K_L K_S$ decays recorded by the KLOE experiment at the DAΦNE e^+e^- collider we have measured the branching fraction for the decay $K_S \rightarrow \pi\mu\nu$. The K_S mesons are identified by the interaction of K_L mesons in the detector. The $K_S \rightarrow \pi\mu\nu$ decays are selected by a boosted decision tree built with kinematic variables and by a time-of-flight measurement. Signal efficiencies are evaluated with data control samples of $K_L \rightarrow \pi\mu\nu$ decays. A fit to the reconstructed muon mass distribution finds 7223 ± 180 signal events. Normalising to the $K_S \rightarrow \pi^+\pi^-$ decay events the result for the branching fraction is $\mathcal{B}(K_S \rightarrow \pi\mu\nu) = (4.56 \pm 0.11_{\text{stat}} \pm 0.17_{\text{syst}}) \times 10^{-4}$. It is the first measurement of this decay mode and the result allows an independent determination of $|V_{us}|$ and a test of the lepton-flavour universality.

Keywords: e^+e^- collisions, K^0 meson, semileptonic decay

1. Introduction

The branching fraction for semileptonic decays of charged and neutral kaons together with the lifetime measurements are used to determine the $|V_{us}|$ element of the Cabibbo–Kobayashi–Maskawa quark mixing matrix. The relation among the matrix elements of the first row, $|V_{ud}|^2 + |V_{us}|^2 + |V_{ub}|^2 = 1$, provides the most stringent test of the unitarity of the quark mixing matrix. Different factors contribute to the uncertainty in determining $|V_{us}|$ from kaon decays [1, 2, 3] and among the six semileptonic decays the contribution of the lifetime uncertainty is smallest for the K_S meson. Nevertheless, given the lack of pure high-intensity K_S meson beams contrary to the case of K^\pm and K_L mesons, the $K_S \rightarrow \pi e \nu$ decay provides the least precise determination of $|V_{us}|$, and the branching fraction $\mathcal{B}(K_S \rightarrow \pi\mu\nu)$ has not yet been measured. Measurement of this decay mode allows an independent determination of $|V_{us}|$ and to extend the test of lepton-flavour universality to K_S semileptonic decays by comparison with the expected value of $(4.69 \pm 0.06) \times 10^{-4}$ [4] derived from $\mathcal{B}(K_S \rightarrow \pi e \nu)$.

We present a measurement of the $K_S \rightarrow \pi\mu\nu$ branching fraction performed by the KLOE experiment at the DAΦNE ϕ -factory of the Frascati National Laboratory based on an integrated luminosity of 1.6 fb^{-1} . DAΦNE [5] is an electron–positron collider running at the centre-of-mass energy of 1.02 GeV colliding e^+ and e^- beams at an angle of $\pi - 0.025$ rad and with a bunch-crossing period of 2.71 ns. The ϕ mesons are produced with a small transverse momentum of 13 MeV and K_L – K_S pairs are produced almost back-to-back with a cross section times the $\phi \rightarrow K_L K_S$ branching fraction of about $1 \text{ } \mu\text{b}$. The beam energy, the energy spread, the beams transverse momentum and the position of the interaction point are measured using Bhabha scattering events [6].

The K_S (K_L) mesons are identified (*tagged*) by the observation of a K_L (K_S) meson in the opposite hemisphere. This tagging procedure allows the selection

efficiency for $K_S \rightarrow \pi\mu\nu$ to be evaluated with good accuracy using a sample of the abundant decay $K_L \rightarrow \pi\mu\nu$ tagged by the detection of $K_S \rightarrow \pi^+\pi^-$ decays. The branching fraction is extracted normalising the number of $K_S \rightarrow \pi\mu\nu$ events to the number of $K_S \rightarrow \pi^+\pi^-$ events recorded in the same dataset.

2. The KLOE detector

The detector¹ consists of a large-volume cylindrical drift chamber, surrounded by a lead/scintillating fibers finely-segmented calorimeter. A superconducting coil around the calorimeter provides a 0.52 T axial magnetic field. The beam pipe at the interaction region is spherical in shape with 10 cm radius, made of a 0.5 mm thick beryllium-aluminum alloy. Final-focus quadrupoles are located at ± 50 cm from the interaction region. Two small lead/scintillating-tile calorimeters [7] are wrapped around the quadrupoles.

The drift chamber [8], 4 m in diameter and 3.3 m long, has 12582 drift cells arranged in 58 concentric rings with alternating stereo angles and is filled with a low-density gas mixture of 90% helium–10% isobutane. The chamber shell is made of carbon fiber-epoxy composite with an internal wall of 1.1 mm thickness at 25 cm radius. The spatial resolution is $\sigma_{xy} = 0.15$ mm and $\sigma_z = 2$ mm in the transverse and longitudinal projections, respectively. The momentum resolution is $\sigma_{p_T}/p_T = 0.4\%$, tracks vertices are reconstructed with a spatial resolution of about 3 mm.

The calorimeter [9] is divided into a barrel and two endcaps and covers 98% of the solid angle. The readout granularity is 4.4×4.4 cm², for a total of 2440 cells arranged in five layers. Each cell is read out at both ends by photomultipliers. The energy deposits are obtained from signal amplitudes while the arrival time and the position along the fibers are obtained from time differences between the two signals. Cells close in time and space are grouped into energy clusters. The cluster energy E is the sum of the cell energies, the cluster time and position are energy-weighted averages. Energy and time resolutions are $\sigma_E/E = 0.057/\sqrt{E \text{ (GeV)}}$ and $\sigma_t = 54 \text{ ps}/\sqrt{E \text{ (GeV)}} \oplus 100 \text{ ps}$, respectively. The cluster spatial resolution is $\sigma_{\parallel} = 1.4 \text{ cm}/\sqrt{E \text{ (GeV)}}$ along the fibers and $\sigma_{\perp} = 1.3 \text{ cm}$ in the orthogonal direction.

The first-level trigger [10] uses both the calorimeter and the drift chamber information; the calorimeter trigger requires two energy deposits with $E > 50$ MeV in the barrel and $E > 150$ MeV in the endcaps; the drift chamber trigger is based on the number and topology of hit drift cells. A second-level cosmic-ray veto rejects events with at least two energy deposits above 30 MeV in the outermost calorimeter layer. The trigger time is determined by the first particle reaching the calorimeter and is synchronised with the DAΦNE radio frequency signal. The time interval between bunch crossings is smaller than the time

¹KLOE uses a coordinate system where the z axis is the bisector of the electron and positron beams, x and y axes define the transverse plane, the polar angle is relative to the z axis.

spread of the signals produced by the particles, thus the time of the bunch crossing originating the event, T_0 , is determined after event reconstruction and all the times related to that event are shifted accordingly. Data for reconstruction are selected by an on-line filter [11] to reject beam backgrounds. The filter also records the events into different output files for analysis according to their properties and topology (event classification), 5% of the events are recorded without applying the filter to control the efficiency of the event classification.

3. Data sample and event preselection

Processes of interest for the analysis are simulated with the GEANFI Monte Carlo (MC) program [11] for an integrated luminosity equal to that of the data. All ϕ decays are generated according to their branching fractions as well as other final states produced in e^+e^- annihilation. The operating conditions of DAΦNE during data taking as well as measurements of beam parameters are included in the MC on a run-by-run basis. Calorimeter energy deposits and drift chamber hits from beam background acquired with a random trigger are overlaid onto the simulated events. The simulated events are processed with the same reconstruction algorithms as the data.

Kaons from ϕ -meson decays are emitted in two opposite hemispheres with mean decay path $\lambda_S = 5.9$ mm and $\lambda_L = 3.4$ m, thus about 50% of K_L mesons reach the calorimeter before decaying. The velocity of the K_L in the ϕ reference system is $\beta^* = 0.22$. K_S mesons are tagged by K_L interactions in the calorimeter, named K_L -crash in the following, with a clear signature of a late signal of about 25 ns not associated to tracks. The following requirements are applied to select K_L -crash:

- a cluster with energy $E_{\text{clu}} > 100$ MeV not associated to tracks (neutral cluster); the centroid of the neutral cluster defines the K_L direction with a resolution of $\sim 1^\circ$;
- polar angle of the neutral cluster $15^\circ < \theta_{\text{clu}} < 165^\circ$ to suppress small-angle beam backgrounds;
- $0.17 < \beta^* < 0.28$ for the velocity in the ϕ reference system of the particle originating the neutral cluster; β^* is obtained from the velocity in the laboratory system, $\beta = r_{\text{clu}}/ct_{\text{clu}}$, with t_{clu} being the cluster time and r_{clu} the distance from the nominal interaction point, the ϕ transverse momentum determined run-by-run and the angle between the ϕ momentum and the K_L -crash direction.

Assuming the neutral kaon mass, the K_S 4-momentum is defined by the K_L -crash direction and the ϕ 4-momentum: $P_{K_S} = P_\phi - P_{K_L}$.

The $K_S \rightarrow \pi\mu\nu$ candidates are selected requiring two tracks of opposite curvature forming a vertex inside the cylinder defined by

$$\rho_{\text{vtx}} = \sqrt{x_{\text{vtx}}^2 + y_{\text{vtx}}^2} < 5 \text{ cm} \quad |z_{\text{vtx}}| < 10 \text{ cm}. \quad (1)$$

In case more than one vertex is found, the closest to the interaction region is chosen. The above requirements define the event preselection.

After preselection, the data sample contains about 300 million events and its composition, as evaluated by simulation, is shown in Table 1. The large majority of events are $K_S \rightarrow \pi^+\pi^-$ decays, and there is also a large contribution from $\phi \rightarrow K^+K^-$ events where one kaon or its decay products generate a fake K_L -crash and the other kaon decays early into $\pi^\pm\pi^0$.

Table 1: Number of data and simulated events after preselection.

	Events [10^3]	Fraction [%]
Data	301646	
MC	312019	
$K_S \rightarrow \pi^+\pi^-$	301976	96.78
$\phi \rightarrow K^+K^-$	9566	3.07
$K_S \rightarrow \pi e \nu$	259	0.08
$K_S \rightarrow \pi \mu \nu$	140	0.04
$K_S \rightarrow \pi^0\pi^0$	30	0.01
Others	47	0.02

The distribution of β^* is shown in Figure 1 for data and simulated events. Two peaks are visible, the first is associated to events triggered by photons or electrons, and the second to events triggered by charged pions. The trigger is synchronised with the bunch crossing and the time difference between a photon (or electron) and a pion (or muon) arriving at the calorimeter corresponds to a time shift of about one bunch-crossing.

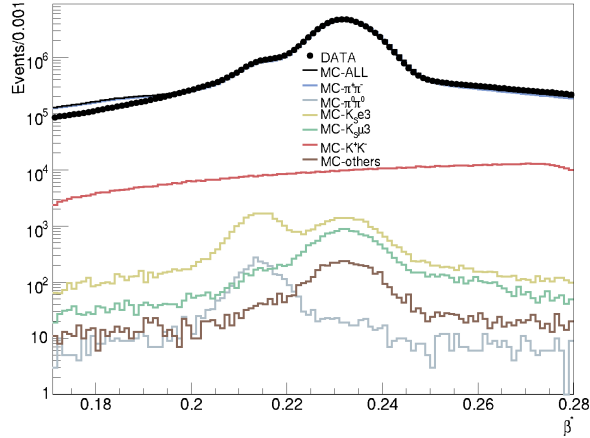


Figure 1: Distribution of β^* after preselection for data and simulated events.

4. Selection of signal and normalisation events

The selection of signal events is performed in two steps; first a selection based on the event kinematics using only tracking variables and then a selection based on the time-of-flight measured with the calorimeter. The two groups of variables are uncorrelated. In order to assign a time to the particles each track is associated to a cluster. The track-to-cluster association (TCA) is applied as follows: for each track connected to the vertex a cluster with $E_{\text{clu}} > 20$ MeV and $15^\circ < \theta_{\text{clu}} < 165^\circ$ is required whose centroid is within 60 cm of the track extrapolation to the calorimeter front surface. The event is retained only if TCA is satisfied by both tracks.

Five variables with good discriminating power against background are used in a multivariate analysis. A boosted decision tree (BDT) classifier is built with the following variables:

\vec{p}_1, \vec{p}_2 : the tracks momenta;

$\alpha_{1,2}$: the angle at the vertex between the two momenta in the K_S reference system;

α_{SL} : the angle between $\vec{p}_{\text{sum}} = \vec{p}_1 + \vec{p}_2$ and the K_L -crash direction;

Δp : the difference between $|\vec{p}_{\text{sum}}|$ and the absolute value $|\vec{p}_{K_S}|$ of the K_S momentum determined using the tagging K_L ;

$m_{\pi\pi}$: the invariant mass reconstructed from \vec{p}_1 and \vec{p}_2 , in the hypothesis of charged-pion mass.

The distributions of the variables are shown in Figure 2 for data and simulated events.

After preselection two cuts are applied to suppress the background in the tails of the distributions:

$$p < 320 \text{ MeV for both tracks} \quad \text{and} \quad \Delta p < 190 \text{ MeV.} \quad (2)$$

The training of the BDT classifier is done on a simulated sample of 5,000 $K_S \rightarrow \pi\mu\nu$ events and a sample of 50,000 background events; samples of the same size are used for the test. After training and test the classification is run on all events of the MC and data sample. The distribution of the BDT classifier output is shown in Figure 3 for data and simulated events. The data distribution is well reproduced by simulation in the region populated by the signal. To suppress the large background of $K_S \rightarrow \pi^+\pi^-$ and $\phi \rightarrow K^+K^-$ events, a cut is applied

$$BDT > 0.18 \quad (3)$$

chosen to maximise the ratio $S/\sqrt{S+B}$ where S and B are the signal and background yields.

The selected events contain $\pi\pi$, $K\pi$, $e\pi$ track pairs for the main backgrounds and $\mu\pi$ for the signal. A selection based on time-of-flight measurement is performed to identify $\mu\pi$ pairs. For each track associated to a cluster, the difference

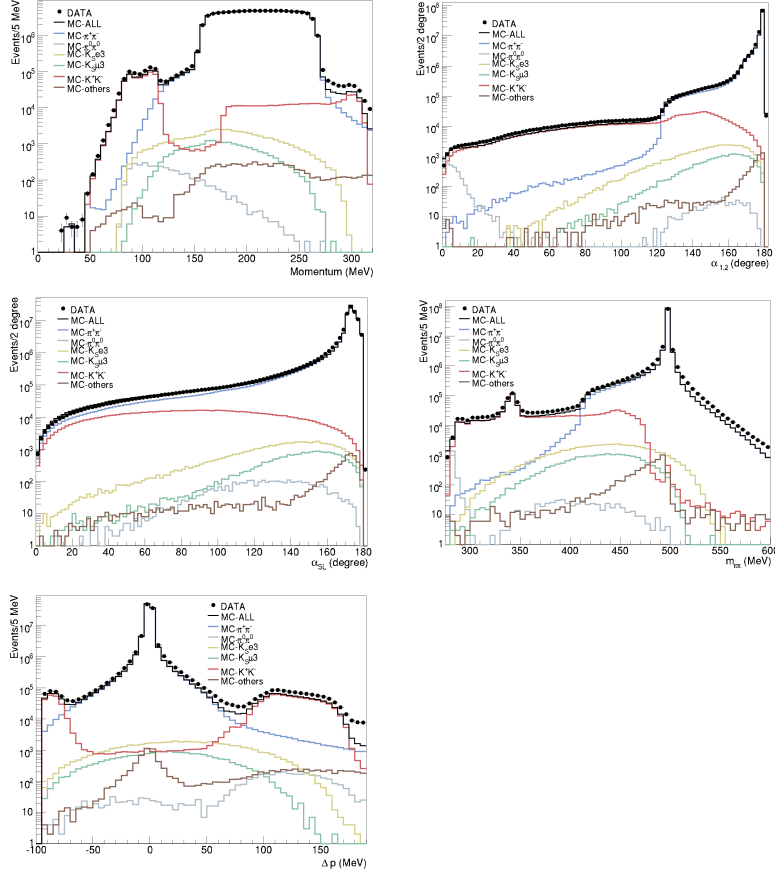


Figure 2: Distributions of the variables used in the multivariate analysis for data and simulated events after preselection. From top left: track momenta (p_1, p_2), angle between the two tracks in the K_S reference system ($\alpha_{1,2}$), angle between K_L and K_S directions (α_{SL}), two-track invariant mass in the hypothesis of charged pions ($m_{\pi\pi}$), $\Delta p = |\vec{p}_{\text{sum}}| - |\vec{p}_{K_S}|$.

between the time measured by the calorimeter and the time-of-flight measured along the particle trajectory

$$\delta t_i = t_{\text{clu},i} - L_i/c\beta_i \quad i = 1, 2$$

is computed, where $t_{\text{clu},i}$ is the time of the cluster associated to track i , L_i is the length of the track, and $\beta_i = p_i/\sqrt{p_i^2 + m_i^2}$ is function of the mass hypothesis for track i . To reduce the uncertainty due to the T_0 determination, the difference

$$\delta t_{1,2} = \delta t_1 - \delta t_2$$

is used to determine the mass assignment to the tracks. The $\pi\pi$ hypothesis is tested first, the distribution of $\delta t_{\pi\pi} = \delta t_{1,\pi} - \delta t_{2,\pi}$ is shown in Figure 4(left).

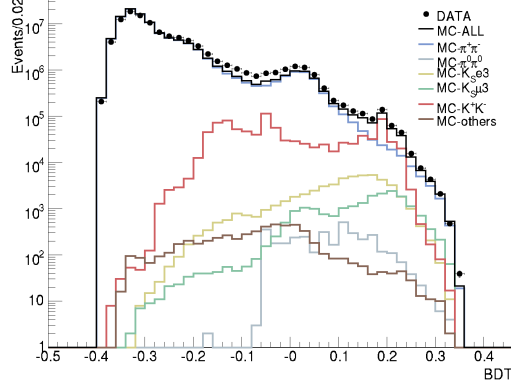


Figure 3: Distribution of the BDT classifier output for data and simulated events.

A fair agreement is observed between data and simulation, the $K_S \rightarrow \pi\mu\nu$ and $K_S \rightarrow \pi e\nu$ distributions are well separated and the K^+K^- background is isolated in the tails of the distribution, however the signal is hidden under a large $K_S \rightarrow \pi^+\pi^-$ background. To reduce the background a cut is applied

$$1 \text{ ns} < |\delta t_{\pi\pi}| < 3 \text{ ns}. \quad (4)$$

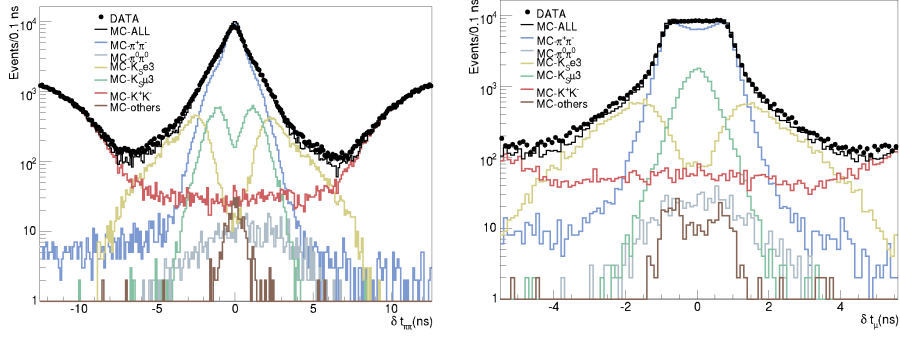


Figure 4: Distributions of $\delta t_{\pi\pi}$ (left) and δt_{μ} (right) for data and simulated events.

The $\pi\mu$ hypothesis is tested by assuming the pion and muon mass for either track

$$\delta t_{\pi\mu} = \delta t_{1,\pi} - \delta t_{2,\mu} \quad \text{and} \quad \delta t_{\mu\pi} = \delta t_{1,\mu} - \delta t_{2,\pi}.$$

The two-dimensional $(\delta t_{\pi\mu}, \delta t_{\mu\pi})$ distribution for simulated signal events shows that the correct mass assignment corresponds to the smaller absolute value of the two hypotheses. The distribution of the signed value of $\delta t_{\mu} = \min[|\delta t_{\pi\mu}|, |\delta t_{\mu\pi}|]$ is shown in Figure 4(right) for data and simulated events. The distribution for

the signal is narrow and peaked at zero while it is broader for the backgrounds. A final cut is applied

$$|\delta t_\mu| < 0.5 \text{ ns.} \quad (5)$$

Table 2: Number of events after the δt_μ selection for data and simulated events.

	Events	Fraction [%]
Data	38686	
MC	36444	
$K_S \rightarrow \pi^+\pi^-$	25853	70.9
$\phi \rightarrow K^+K^-$	475	1.30
$K_S \rightarrow \pi e \nu$	448	1.23
$K_S \rightarrow \pi \mu \nu$	9424	25.9
Others	244	0.7

The number of surviving events in the data sample is 38686 and its composition as evaluated by simulation is listed in Table 2. After the mass assignment to the two tracks the invariant mass of the charged particle identified as the muon is evaluated as

$$m_\mu^2 = (E_{K_S} - E_\pi - p_{\text{miss}})^2 - p_\mu^2$$

with $p_{\text{miss}}^2 = (\vec{p}_{K_S} - \vec{p}_\pi - \vec{p}_\mu)^2$, E_{K_S} and \vec{p}_{K_S} being the energy and momentum reconstructed using the tagging K_L , and \vec{p}_π , \vec{p}_μ , the momenta of the candidate pion and muon track.

The number of signal events is extracted with a fit to the m_μ^2 distribution with the MC shapes of three components: $K_S \rightarrow \pi \mu \nu$, $K_S \rightarrow \pi^+\pi^-$ and the sum of all other backgrounds. The fit is performed in the range $-6000 < m_\mu^2 < 24000$ MeV^2 with 48 degrees of freedom. The third component, which is peaked around m_e^2 , is constrained to a negligible value by the fit. Figure 5 shows the distribution of m_μ^2 for data, simulated events and the fit, and Table 3 presents the result of the fit. The number of signal events is

$$N_{\pi\mu\nu} = 7223 \pm 180 \quad \text{with } \chi^2/\text{ndf} = 30/48.$$

Table 3: Result of the fit to the m_μ^2 distribution.

	Fraction	Events
$\pi\mu\nu$	0.23	7223 ± 180
$\pi^+\pi^-$	0.77	23764 ± 270
Total		30987

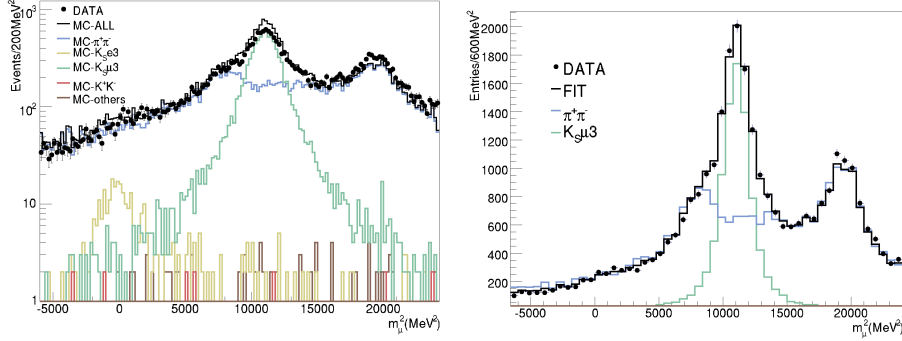


Figure 5: The m_μ^2 distribution for data, MC signal and background (left); comparison of data with the fit (right).

The normalisation sample of $K_S \rightarrow \pi^+\pi^-$ events is selected by requiring $140 < p < 280$ MeV for both tracks (Figure 2). This requirement selects $N_{\pi\pi} = (282.314 \pm 0.017) \times 10^6$ events with a purity of 99.9% as determined by simulation.

5. Determination of efficiencies

The branching fraction for the $K_S \rightarrow \pi\mu\nu$ decay is evaluated as

$$\mathcal{B}(K_S \rightarrow \pi\mu\nu) = \frac{N_{\pi\mu\nu}}{\epsilon_{\pi\mu\nu}} \times \frac{\epsilon_{\pi\pi}}{N_{\pi\pi}} \times R_\epsilon \times \mathcal{B}(K_S \rightarrow \pi^+\pi^-), \quad (6)$$

where $N_{\pi\mu\nu}$ and $N_{\pi\pi}$ are the numbers of $K_S \rightarrow \pi\mu\nu$ and $K_S \rightarrow \pi^+\pi^-$ events, $\epsilon_{\pi\mu\nu}$ and $\epsilon_{\pi\pi}$ are the respective selection efficiencies, and R_ϵ is the ratio of the efficiencies for the trigger, on-line filter and preselection for the two decays.

The signal selection efficiency is determined with $K_L \rightarrow \pi\mu\nu$ control samples (CS) and evaluated as

$$\epsilon_{\pi\mu\nu} = \epsilon_{\text{CS}} \times \frac{\epsilon_{\pi\mu\nu}^{\text{MC}}}{\epsilon_{\text{CS}}^{\text{MC}}}, \quad (7)$$

where ϵ_{CS} is the efficiency of the control sample and $\epsilon_{\pi\mu\nu}^{\text{MC}}$, $\epsilon_{\text{CS}}^{\text{MC}}$ are the efficiencies obtained from simulation for the signal and control samples, respectively.

The $K_L \rightarrow \pi\mu\nu$ decay [12, 13] is kinematically identical to the signal, the only difference being the much longer decay path. For the control sample the tagging is done with $K_S \rightarrow \pi^+\pi^-$ decays, preselected in the same way as for the signal sample with the additional cut $|m_{\pi\pi} - m_{K^0}| < 15$ MeV to increase the purity. The radial distance of the K_L vertex is required to be smaller than 5 cm to match the signal selection, but greater than 1 cm to minimise the ambiguity in identifying the K_L and K_S vertices. The control sample is composed mainly of $K_L \rightarrow \pi e \nu$, $K_L \rightarrow \pi^+\pi^-\pi^0$ and $K_L \rightarrow \pi\mu\nu$ decays, while most of $K_L \rightarrow \pi^0\pi^0\pi^0$ decays are rejected by the requirement of two tracks.

The distribution of the missing mass, m_{miss}^2 , of the two tracks connected to the K_L vertex, assigning the charged-pion mass, shows a narrow isolated peak at the π^0 mass; a cut $m_{\text{miss}}^2 < 15000 \text{ MeV}^2$ efficiently rejects the $K_L \rightarrow \pi^+\pi^-\pi^0$ decays. The number of events in the control sample is 911757.

In order to evaluate the signal selection efficiency, two control samples are used, one selected based on kinematic variables and the other based on time-of-flight (TOF), the two groups of variables being largely uncorrelated.

The control sample for evaluating the efficiencies of the selection with kinematic variables and BDT classifier is selected applying a cut on the two-dimensional $(\delta t_{\pi\mu}, \delta t_{\mu\pi})$ distribution that removes most of the $K_L \rightarrow \pi e \nu$ events. The purity of the sample as determined with simulation is 86%. The resolutions in the measurement of the tagging K_S (control sample) are similar to those of the tagging K_L (signal sample) and the same BDT classifier is used for both samples. The BDT MC distributions for the signal and control sample are compared in Figure 6(left). Applying to the control sample the same selections as for the signal, the efficiencies evaluated with Eq. (7) are

$$\epsilon(\text{kinem. sel.}) = 0.982 \pm 0.004_{\text{stat}} \quad \text{and} \quad \epsilon(\text{BDT}) = 0.417 \pm 0.003_{\text{stat}}.$$

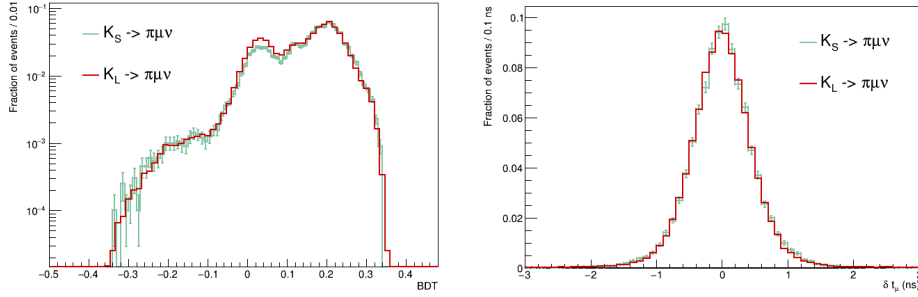


Figure 6: Normalised Monte Carlo distributions of the BDT classifier output (left) and δt_{μ} (right) for $K_L \rightarrow \pi\mu\nu$ and $K_S \rightarrow \pi\mu\nu$ events.

To evaluate TCA and TOF efficiencies for the signal, the T0 determination using the earlier among the two clusters associated with the K_S decay has to be considered. The control sample selection therefore requires the earliest cluster to be associated with one of charged secondary particles from K_L decay and a cut on the $(m_{\pi\pi}, m_{\text{miss}}^2)$ distribution to reject $K_L \rightarrow \pi e \nu$ events. The purity of the sample as determined with simulation is 87%. The MC distributions of δt_{μ} for the signal and control sample are compared in Figure 6(right). Applying to the control sample the analysis procedure as for the signal the efficiencies evaluated with Eq. (7) are

$$\epsilon(\text{TCA}) = 0.347 \pm 0.002_{\text{stat}} \quad \text{and} \quad \epsilon(\text{TOF}) = 0.392 \pm 0.003_{\text{stat}}.$$

The correction factors in Eq. (7) differ from one by less than 10% but for $\epsilon(\text{TOF})$ where it differs by 20%.

The tails of the m_μ^2 distribution in Figure 5(left) are not included in the fit to improve its stability, the relative efficiency is 0.991 ± 0.001 .

The signal selection efficiencies are summarised in Table 4 where only the statistical errors are shown. Combining the values accounting for the correlation of the control samples we obtain $\epsilon_{\pi\mu\nu} = 0.0552 \pm 0.0005$.

Table 4: Efficiencies for the signal selections. The errors are statistical, the error of the total efficiency accounts for the correlation of the control samples.

Selection	Efficiency
Kinematic selection	0.982 ± 0.004
BDT selection	0.417 ± 0.003
TCA selection	0.347 ± 0.002
TOF selection	0.392 ± 0.003
FIT range	0.991 ± 0.001
Total	0.0552 ± 0.0005

The ratio R_ϵ in Eq. (6) accounts for several effects all depending on the global properties of the event: trigger, on-line filter, event classification, T_0 determination, K_L -crash and K_S identification. The various contributions to R_ϵ evaluated with simulation are listed in Table 5 where only the statistical errors are shown.

Table 5: Contributions to the ratio of efficiencies R_ϵ in Eq. (6). The error on R_ϵ is calculated as the quadratic sum of the errors of the single ratios.

Selection	R_ϵ
Trigger	1.0649 ± 0.0005
On-line filter	1.0113 ± 0.0002
Event classification	1.1406 ± 0.0007
T_0 determination	1.0135 ± 0.0002
K_L -crash and β^*	1.1283 ± 0.0022
K_S identification	1.0481 ± 0.0012
R_ϵ	1.472 ± 0.004

The efficiency of the $K_S \rightarrow \pi^+\pi^-$ normalisation sample is measured using the preselected data by varying the cut on the vertex transverse position, as in Eq. (1), in 1 cm steps from $\rho_{\text{vtx}}^{\text{max}} = 1$ cm to $\rho_{\text{vtx}}^{\text{max}} = 4$ cm, based on the observation that ρ_{vtx} and the tracks momenta are very loosely correlated. Using Eq. (7) and extrapolating to $\rho_{\text{vtx}}^{\text{max}} = 5$ cm the efficiency is $\epsilon_{\pi\pi} = (96.569 \pm 0.004)\%$. Alternatively, the efficiency is evaluated using the $K_S \rightarrow \pi^+\pi^-$ data sample (with $\rho_{\text{vtx}}^{\text{max}} = 5$ cm): $\epsilon_{\pi\pi} = (96.657 \pm 0.002)\%$. The latter value is used as the efficiency and the difference between the two values is taken as systematic

uncertainty. The number of $K_S \rightarrow \pi^+\pi^-$ events corrected for the efficiency is

$$N_{\pi\pi}/\epsilon_{\pi\pi} = (292.08 \pm 0.27) \times 10^6.$$

6. Systematic uncertainties

Three main systematic uncertainties affect the signal count: BDT and time-of-flight selection, and the m_μ^2 fit.

The distributions of the BDT classifier output for the data and simulated signal and control sample events are in good agreement as shown in Figures 3 and 6. The resolution of the BDT variable predicted by simulation comparing the reconstructed events with those at generation level is $\sigma_{\text{BDT}} = 0.005$. The analysis is repeated varying the BDT cut of Eq. (3), the number of signal events is found to be stable and the rms value of the differences corresponds to a relative uncertainty of 0.3%.

The main source of uncertainty in the TOF selection is the cut on $\delta t_{\pi\pi}$ in Eq. (4) because the signal and background distributions in Figure 4(left) are steep and with opposite slopes; the subsequent selection on δt_μ in Eq. (5) has a minor effect. The resolution of the $\delta t_{\pi\pi}$ variable evaluated with simulation and $K_S \rightarrow \pi^+\pi^-$ data control samples is 0.27 ns. The analysis is repeated varying the $\delta t_{\pi\pi}$ lower cut in the range 0.5–1.25 ns, the rms value of the differences corresponds to a relative uncertainty of 3.0%. This is the main systematic uncertainty affecting the measurement.

The fit to the m_{μ^2} distribution in Figure 5 is repeated varying the range and the bin size. The relative systematic uncertainty on the number of events is 0.3% obtained shifting the range by five bins on either side and increasing the bin size by a factor of two.

The statistical uncertainties of the simulation signal and control samples, and of the data control sample contribute with a relative uncertainty of 0.8% (Table 4).

The dependence of R_ϵ on systematic effects has been studied in previous analyses for different K_S decays selected with the K_L -crash method: $K_S \rightarrow \pi^+\pi^-$ and $K_S \rightarrow \pi^0\pi^0$ [14], and $K_S \rightarrow \pi e \nu$ [15]. The systematic uncertainties are evaluated by a comparison of data with simulation, as described in the following.

Trigger – Two triggers are used for recording the events, the calorimeter trigger and the drift chamber trigger. The validation of the MC relative efficiency is derived from the comparison of the single-trigger and coincidence rates with the data. The data over MC ratio is 0.999 with negligible error.

On-line filter and event classification – The event classification produces different streams for the analyses. The $K_L K_S$ stream selects events based on the properties of K_S and K_L decays. In more than 99% of the cases the events are selected based on the K_S decay topology and the K_L -crash signature and differences between MC and data are accounted for in the systematic uncertainties derived below for the K_S identification and K_L -crash.

T₀ – The systematic uncertainty is evaluated analysing the data and MC T₀ distributions for the decays with the most different timing properties: $K_S \rightarrow \pi^+\pi^-$ and $K_S \rightarrow \pi^0\pi^0$ [14]. The data over MC ratios is one with an uncertainty of less than 0.1%.

K_L-crash and β^* selection – The systematic uncertainty is evaluated comparing data and simulated events tagged by $K_S \rightarrow \pi^+\pi^-$ and $K_S \rightarrow \pi^0\pi^0$ decays which have different timing and topology characteristics. The data over MC ratio is 1.001 with negligible error.

K_S identification – The systematic uncertainty due to the requirement of two tracks forming a vertex in the cylinder defined by Eq. (1) is evaluated separately for signal and normalisation samples. The first is evaluated with $K_L \rightarrow \pi\mu\nu$ events selected with the same vertex requirements as for the signal but tagged by $K_S \rightarrow \pi^0\pi^0$ decays. For the $K_S \rightarrow \pi^+\pi^-$ sample the efficiency is evaluated by tagging with K_L -crash and removing the requirement of the vertex. Combining the two values gives a data over MC ratio of 1.002 ± 0.017 where the error is due to the purity of the samples.

The R_ϵ total systematic uncertainty is estimated by combining the data over MC ratios and amounts to 1.7%.

Including the systematic uncertainties the factors in Eq. (6) are:

$$\epsilon_{\pi\mu\nu} = 0.0552 \pm 0.0017 \quad \text{and} \quad R_\epsilon = 1.472 \pm 0.025.$$

All systematic uncertainties are summarised in Table 6.

Table 6: Summary of systematic uncertainties of $\epsilon_{\pi\pi}$, $\epsilon_{\pi\mu\nu}$ and R_ϵ .

Source	$\epsilon_{\pi\pi}$ [%]	$\epsilon_{\pi\mu\nu}$ [%]	R_ϵ [%]
$K_S \rightarrow \pi^+\pi^-$ selection	0.1		
BDT selection		0.3	
TOF selection		3.0	
Fit m_μ^2 distribution		0.3	
MC and data CS statistics		0.8	
Trigger			0.1
T ₀ determination			<0.1
K_L -crash and β^*			0.1
K_S identification			1.7
Total	0.1	3.1	1.7

7. Result

From Eq. (6) with $N_{\pi\mu\nu} = 7223 \pm 180$, $N_{\pi\pi}/\epsilon_{\pi\pi} = (292.08 \pm 0.27) \times 10^6$, the values of the efficiencies $\epsilon_{\pi\mu\nu} = 0.0552 \pm 0.0017$, $R_\epsilon = 1.472 \pm 0.025$, and the

value $\mathcal{B}(K_S \rightarrow \pi^+\pi^-) = 0.69196 \pm 0.00051$ measured by KLOE [15], we derive the branching fraction

$$\mathcal{B}(K_S \rightarrow \pi\mu\nu) = (4.56 \pm 0.11_{\text{stat}} \pm 0.17_{\text{syst}}) \times 10^{-4} = (4.56 \pm 0.20) \times 10^{-4}.$$

This is the first measurement of this decay mode and completes the set of kaon semileptonic decays. The branching fraction for $K_S(K_L) \rightarrow \pi\ell\nu$ decay is related to the weak coupling constant and V_{us} through the relation

$$\mathcal{B}(K_S \rightarrow \pi\ell\nu) = \frac{G^2 |f_+(0)V_{us}|^2}{192\pi^3} \tau_s m_K^5 I_K^\ell S_{\text{EW}} (1 + \delta_{\text{EM}}^{K\ell})^2 \quad (8)$$

where $f_+(0)$ is the hadronic form factor at zero momentum transfer, m_K and τ_s are the K_S mass and lifetime, I_K^ℓ is the phase space integral, S_{EW} is the short-distance electroweak correction [17] and $\delta_{\text{EM}}^{K\ell}$ is the long-distance electromagnetic correction [18, 19]. Assuming universality of the kaon-lepton coupling the expected value [4] is

$$\mathcal{B}(K_S \rightarrow \pi\mu\nu)_{\text{PDG}} = \mathcal{B}(K_S \rightarrow \pi e\nu) \times R(I_K^\ell) \times \frac{(1 + \delta_{\text{EM}}^{K\mu})^2}{(1 + \delta_{\text{EM}}^{Ke})^2} = (4.69 \pm 0.06) \times 10^{-4}$$

as derived from the value of the branching fraction $\mathcal{B}(K_S \rightarrow \pi e\nu)$ measured by KLOE [15] and the ratio $R(I_K^\ell)$ of the phase space integrals for the semileptonic decays $K_L \rightarrow \pi\mu\nu$ and $K_L \rightarrow \pi e\nu$ measured by KTeV [16].

Inverting Eq. (8) and using $I_K^\mu = 0.10262 \pm 47$ [3] we derive

$$|f_+(0)V_{us}|_{K_S \rightarrow \pi\mu\nu} = 0.2126 \pm 0.0046.$$

The ratio to the value for $K_S \rightarrow \pi e\nu$ decay, $|f_+(0)V_{us}|_{K_S \rightarrow \pi e\nu} = 0.2153 \pm 14$ [3], allows to confirm the assumption of kaon-lepton coupling universality

$$r_{\mu e} = \frac{|f_+(0)V_{us}|_{K_S \rightarrow \pi\mu\nu}^2}{|f_+(0)V_{us}|_{K_S \rightarrow \pi e\nu}^2} = 0.975 \pm 0.044.$$

These results are consistent with those determined for the other kaon semileptonic decays [1, 3] though less precise mainly due to the intrinsic limitations related to μ - π discrimination in the momentum range 100–250 MeV.

8. Conclusion

A measurement of the branching fraction for the decay $K_S \rightarrow \pi\mu\nu$ is presented based on data collected with the KLOE experiment at the DAΦNE e^+e^- collider corresponding to an integrated luminosity of 1.6 fb^{-1} . The $\phi \rightarrow K_L K_S$ decays are exploited to select samples of pure and quasi-monochromatic K_S mesons and data control samples of $K_L \rightarrow \pi\mu\nu$ decays. The $K_S \rightarrow \pi\mu\nu$ decays are selected by a boosted decision tree built with kinematic variables and by a measurement of time-of-flight. The efficiencies for detecting the $K_S \rightarrow \pi\mu\nu$ decays are derived from $K_L \rightarrow \pi\mu\nu$ data control samples. A fit to the m_μ^2

distribution finds 7223 ± 180 signal events. Normalising to $K_S \rightarrow \pi^+\pi^-$ decay events, the result for the branching fraction is $\mathcal{B}(K_S \rightarrow \pi\mu\nu) = (4.56 \pm 0.11_{\text{stat}} \pm 0.17_{\text{syst}}) \times 10^{-4}$ to be compared with the expected value of $(4.69 \pm 0.06) \times 10^{-4}$ assuming lepton-flavour universality.

Acknowledgements – We warmly thank our former KLOE colleagues for the access to the data collected during the KLOE data taking campaign. We thank the DAΦNE team for their efforts in maintaining low background running conditions and their collaboration during all data taking. We thank our technical staff: G.F. Fortugno and F. Sborzacchi for their dedication in ensuring efficient operation of the KLOE computing facilities; M. Anelli for his continuous attention to the gas system and detector safety; A. Balla, M. Gatta, G. Corradi and G. Papalino for electronics maintenance; C. Piscitelli for his help during major maintenance periods. This work was supported in part by the Polish National Science Centre through the Grants No. 2013/11/B/ST2/04245, 2014/14/E/ST2/00262, 2014/12/S/ST2/00459, 2016/21/N/ST2/01727, 2016/23/N/ST2/01293, 2017/26/M/ST2/00697.

References

- [1] M. Antonelli et al., An evaluation of $|V_{us}|$ and precise tests of the Standard Model from world data on leptonic and semileptonic kaon decays, *Eur. Phys. J. C* **69** (2010) 399, arXiv:1005.2323 [hep-ph].
- [2] M. Moulson, Experimental determination of V_{us} from kaon decays, *PoS CKM2016* (2017) 033, arXiv:1704.04104 [hep-ex].
- [3] F. Ambrosino et al., $|V_{us}|$ and lepton universality from kaon decays with the KLOE detector, *JHEP* **04** (2008) 059, arXiv:hep-ex/0802.3009.
- [4] M. Tanabashi et al. (Particle Data Group), The Review of Particle Physics, *Phys. Rev. D* **98** (2018) 030001.
- [5] A. Gallo et al., DAΦNE Status Report, European Particle Accelerator Conference, 26-30 June 2006, Edinburgh, Scotland, *Conf. Proc. C060626* (2006) 604.
- [6] F. Ambrosino et al., Measurement of the DAΦNE luminosity with the KLOE detector using large angle Bhabha scattering, *Eur. Phys. J. C* **47** (2006) 589, arXiv:hep-ex/0604048.
- [7] M. Adinolfi et al., The QCAL tile calorimeter of KLOE, *Nucl. Instrum. Meth. A* **483** (2002) 649.
- [8] M. Adinolfi et al., The tracking detector of the KLOE experiment, *Nucl. Instrum. Meth. A* **488** (2002) 51.
- [9] M. Adinolfi et al., The KLOE electromagnetic calorimeter, *Nucl. Instrum. Meth. A* **482** (2002) 364.
- [10] M. Adinolfi et al., The trigger system of the KLOE experiment, *Nucl. Instrum. Meth. A* **492** (2002) 134.

- [11] F. Ambrosino et al., Data handling, reconstruction and simulation for the KLOE experiment, Nucl. Instrum. Meth. A **534** (2004) 403, arXiv:physics/0404100.
- [12] F. Ambrosino et al., Measurements of the absolute branching ratios for the dominant K_L decays, the K_L lifetime and V_{us} with the KLOE detector, Phys. Lett. B **632** (2006) 43, arXiv:hep-ex/0509045.
- [13] F. Ambrosino et al., Measurement of the $K_L \rightarrow \pi\mu\nu$ form factor parameters with the KLOE detector, JHEP **12** (2007) 105, arXiv:0710.4470 [hep-ex].
- [14] F. Ambrosino et al., Precise measurement of $\Gamma(K_S \rightarrow \pi^+\pi^-(\gamma))/\Gamma(K_S \rightarrow \pi^0\pi^0)$, with the KLOE detector at DAΦNE, Eur. Phys. J. C **48** (2006) 767, arXiv:hep-ex/0601025.
- [15] F. Ambrosino et al., Study of the branching ratio and charge asymmetry for the decay $K_S \rightarrow \pi e\nu$ with the KLOE detector, Phys. Lett. B **636** (2006) 173, arXiv:hep-ex/0601026.
- [16] T. Alexopoulos et al., Measurements of semileptonic K_L decay form factors, Phys. Rev. D **70** (2004) 092007, arXiv:hep-ex/0406003.
- [17] W. J. Marciano and A. Sirlin, Radiative corrections to $\pi_{\ell 2}$ decays, Phys. Rev. Lett. **71** (1993) 3629.
- [18] V. Cirigliano, M. Giannotti and H. Neufeld, Electromagnetic effects in $K_{\ell 3}$ decays, JHEP **11** (2008) 006, arXiv: 0807.4507 [hep-ph]
- [19] T. C. André, Radiative corrections in $K_{\ell 3}^0$ decays, Annals Phys. **332** (2007) 2518, arXiv:hep-ph/0406006.